Journal of Alloys and Compounds 864 (2021) 158617

Contents lists available at ScienceDirect

Journal of Alloys and Compounds

journal homepage: www.elsevier.com/locate/jalcom

The crystal structures and magnetic properties of TiFeSi coexisting in hexagonal and orthorhombic symmetries

Madalynn Marshall[a], Jasmine Sanford[b], William Shelton[c], Weiwei Xie[a,*]

[a] Department of Chemistry and Chemical Biology, Rutgers University, Piscataway, NJ 08854, USA
[b] Department of Chemistry, Louisiana State University, Baton Rouge, LA 70803, USA
[c] Cain Department of Chemical Engineering, Louisiana State University, Baton Rouge, LA 70803, USA

ARTICLE INFO

Article history:
Received 10 October 2020
Received in revised form 7 December 2020
Accepted 31 December 2020
Available online 10 January 2021

Keywords:
Intermetallics
Magnetism
First-principles calculation

ABSTRACT

The intertwisted helix framework of the chiral FeSi-type structure with the space group $P2_13$ (S.G. $P2_13$) inspired us to investigate other non-centrosymmetric compounds, particularly 111-type phases with different FeSi frameworks. Various FeSi-containing 111-type phases have been summarized according to their valence electron counts and space group. In this work we have focused on the non-centrosymmetric TiFeSi phase. The crystal structure analysis of the hexagonal Fe_2P-type and the reported orthorhombic TiFeSi-type (α-TiFeSi) indicate a superlattice relationship exists between the two structures, which drove us to perform the total energy calculations of the hexagonal and orthorhombic models of TiFeSi. Following the theoretical predictions, a hexagonal TiFeSi phase (β-TiFeSi) is proposed and successfully synthesized at high temperature using arc melting. The crystal structure of the high-temperature hexagonal phase was determined by powder and single crystal X-ray diffraction. After the annealing of the arc-melted samples, TiFeSi crystallizes into an orthorhombic structure with the space group *Ima2*. The systematic magnetic characterizations indicate ferromagnetic properties are present in the non-centrosymmetric orthorhombic α-TiFeSi phase with possible helical magnetic ordering at low temperatures. Moreover, to compare with the centrosymmetric cases, the electronic and magnetic properties of the antiferromagnetic TiNiSi-type MFeSi (M = Zr and Hf) compounds were also examined using both density functional theory and experimental magnetic measurements.

1. Introduction

Primitive cubic FeSi, a chiral structure (*B20* phase, S.G.198), has attracted the interest of scientists for many years after being reported as the first Kondo insulator without rare-earth elements [1,2]. $Fe_{1-x}Co_xSi$, made by doping electrons into FeSi, exhibits half-metallic properties and unusual magnetoresistance [3–5], making it a potential material for spintronic applications. Moreover, the chiral FeSi-type structure is also well-known for hosting a magnetic skyrmion lattice, such as in $Mn_{1-x}T_xSi$ (T = Fe, Co, Ir)[3,6]. As a kind of quasiparticle, the skyrmion can be interpreted as a small perturbation to a uniform magnet. A point-like region, of only a few nanometers in size, can be observed with reversed magnetization expanded with a twist of spins [7,8]. This type of magnetic structure has been proposed as a possible mechanism for the storage of information within an exceptionally small size, only requiring a small amount of energy to do so. It is well accepted by the scientific community that the chiral cubic structures, especially those of $P2_13$ FeSi-type, with the addition of a small external magnetic field have a higher potential to host a skyrmion lattice [9]. However, a new class of chiral material, β-Mn-type Co-Zn-Mn, was discovered to host a magnetic skyrmion lattice above room temperature [10–12]. In addition to the specific structural features, the helical magnetic ordering at zero applied magnetic field is always observed to accompany the skyrmion lattice [13,14].

To explore more possible compounds that host skyrmion lattices, we have focused on the 111-type candidates with both a helical magnetic ordering and a FeSi framework. 111-type compounds, such as the half-Heusler phases, can be well understood using electron counting rules for chemical stability: 18 valence electrons are required to fill the 1 × *s*, 3 × *p*, and 5 × *d* bonding orbitals, leaving the antibonding states empty and leading to a chemically stable material with a direct or pseudo band gap between the filled and empty states [15,16]. However, few experimental investigations of the 18-*n* 111-type have been reported. Among them, the TiNiSi-type MFeSi

* Corresponding author.
E-mail address: weiwei.xie@rutgers.edu (W. Xie).

https://doi.org/10.1016/j.jallcom.2021.158617
0925-8388/

(T = Zr and Hf) compounds attracted our attention due to the relatively isolated FeSi framework [17,18]. Since a vast majority of the structures exhibiting helimagnetic behavior are non-centrosymmetric compounds due to the presence of the Dzyaloshinskii-Moriya interaction [19], TiFeSi presented a higher potential for the targeted behavior than the centrosymmetric TiNiSi-type structure and, therefore, was investigated in detail. The orthorhombic structure of TiFeSi displays a superlattice relationship with a hexagonal Fe_2P-type motif with the non-centrosymmetric space group *P*-62*m* [20]. The stability of the orthorhombic TiFeSi (α-TiFeSi) structure has been the subject of previous research [20]. With the realization of the structural connections, we set out to calculate the total energy of the two phases in order to determine whether the hexagonal TiFeSi (β-TiFeSi) could be achieved under mild synthetic conditions. Such a coexistence has been observed and explained in MnPtSi from the chemical bonding aspects by Grin's group in 2019 [21].

Confirming our calculations, here we report our observation of a new hexagonal phase of TiFeSi (β-TiFeSi) synthesized at high temperature. Furthermore, the magnetic properties of orthorhombic TiFeSi (α-TiFeSi) were studied systematically and the results indicate a ferromagnetic ordering in the non-centrosymmetric compound with a possible helimagnetism at low temperature. Additionally, the MFeSi (M = Zr and Hf) compounds were synthesized and their magnetic behavior was investigated in order to compare the behavior (antiferromagnetic) exhibited by centrosymmetric compounds.

2. Experimental details

2.1. Synthesis

Polycrystalline samples of hexagonal TiFeSi were obtained by arc melting of the elemental metals under an argon atmosphere on a water-cooled stage using a tungsten electrode. Stoichiometric amounts of Ti (pieces, Alfa Aesar 99.9%), Fe (shot, Alfa Aesar 99.97 + %) and Si (pieces, Alfa Aesar 99.9999%) were weighted out (total ~200 mg). A 3% excess of Si was added to compensate for any loss during the arc melting process. The product was turned and melted 5–10 times to ensure good homogeneity in the samples. Throughout every trial, weight losses in total were less than 2%. The repeated arc melting process resulted in the high-temperature hexagonal phase as the majority phase with some orthorhombic phase remaining in the sample.

As-cast samples were placed in Ta foil and annealed at 1000 °C for seven days in an evacuated sealed quartz tube leading a structural change to the orthorhombic phase. Both hexagonal and orthorhombic TiFeSi appear to be stable in air and moisture after being exposed to the air for one week.

2.2. Phase identification

Samples were analyzed for phase identification and purity using a Rigaku MiniFlex 600 powder X-ray diffractometer equipped with Cu K_α radiation (λ = 1.5406 Å, Germanium monochromator). Powder XRD samples were prepared by finely grinding the compounds using a mortar and pestle and placing the powder on top of a grease coated glass slide without any pressure to prevent any preferred orientation. Scans were collected at the Bragg angle (2θ) range of 5–90º in a 0.01º step mode. To confirm the existence of hexagonal phase, the high-resolution synchrotron powder X-ray diffraction at room temperature was collected from the grinded as-cast TiFeSi sample using beamline 11-BM at the Advanced Photon Source, Argonne National Laboratory. A Rietveld profile fit was carried out using Fullprof to obtain the refined structural information [22].

2.3. Crystal structure determination

Single crystals of the TiFeSi samples found among the ground arc melted samples were analyzed using a Bruker Apex II diffractometer with Mo radiation ($\lambda_{K\alpha}$ = 0.71073 Å). Small crystals (~0.01 × 0.01 × 0.01 mm^3) were chosen and mounted on the tip of a Kapton loop. Reflections were collected with an exposure time of 10 s per frame with 0.5° scans in ω with a 2θ ranging from 3° to 70° at 300 K. Over ten different crystals were tested to obtain reliable lattice parameters. The data acquisition, extraction of intensity and correction for Lorentz and polarization effects were performed using Bruker SMART software [23]. The crystal structures were solved with the SHELXTL package [24], using direct methods and refined by full-matrix least-squares on F^2 [24].

2.4. Chemical analysis

Scanning Electron Microscope-Energy-dispersive X-ray spectroscopy (SEM-EDS) was performed with a high vacuum scanning electron microscope (JSM-6610 LV). Samples were placed on carbon tape prior to loading into the SEM chamber. Multiple points and areas were examined for each sample. The samples were examined at 15 kV and the spectra were collected for 100 s to get the chemical composition with via TEAM EDAX software.

2.5. Magnetic properties measurements

Investigation of the temperature dependent magnetic susceptibility of the orthorhombic phase of TiFeSi (α-TiFeSi) and MFeSi (M = Zr, Hf) were carried out on a superconducting quantum interference device (SQUID) magnetometer (Quantum Design, MPMS 7-T) between 2 and 350 K in a 1 T field for TiFeSi and 500 Oe field for the MFeSi samples (up to 390 K for those samples). Each sample (~50 mg) was placed in a gel capsule for measurement. The sample was cooled to 2 K in the absence of field to perform zero-field cooling measurements.

2.6. Total energy and electronic structure calculations

The electronic structures of both hexagonal and orthorhombic structures of TiFeSi were calculated using the full-potential linearized augmented plane wave and local orbitals basis WIEN2k code [25]. Experimental lattice parameters from the single crystal diffraction refinement were used in the calculations. The *c*/*a* ratio in the hexagonal model and *c*/*b*, *c*/*a* ratios in the orthorhombic model were fixed during the volume optimization. The total energies of the two models were fitted with the Birch–Murnaghan equation of state [26].

The electronic and possible magnetic structures of MFeSi (M = Zr and Hf) were also calculated with a WIEN2k package based on the Density Functional Theory (DFT) using projector augmented-wave (PAW) pseudo potentials[27] that were adopted with the Perdew-Burke-Ernzerhof generalized gradient approximation (PBE-GGA) [28]. Exchange and correlation were treated by the local density approximation (LDA) and the local spin density approximation (LSDA) [29]. Spin-orbit coupling was included. The energy cutoff was set at 500 eV. Reciprocal space integrations were completed over an 12 × 12 × 6 Monkhorst-Pack *k*-points mesh with the linear tetrahedron method [30]. With these settings, the calculated total energy converged to less than 0.1 meV per atom.

3. Results and discussion

3.1. FeSi-helix structure and 111 phases

Our investigation was motivated by the particularity of the FeSi structure. FeSi crystallizes into a primitive cubic structure (S.G.

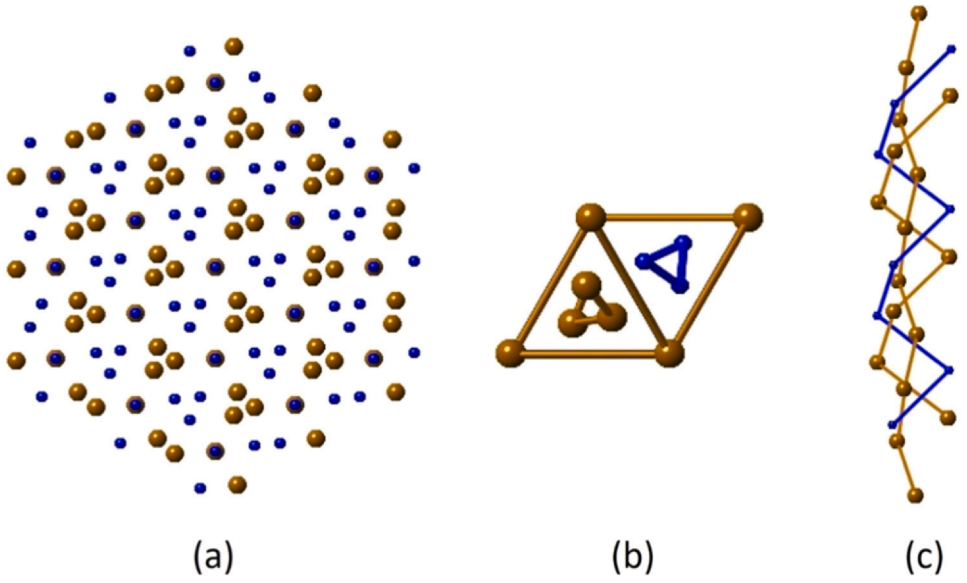

Fig. 1. (a) View along < 111 > of FeSi (taking 3 unit cells along each axis), (b) Two neighboring helical structures with Fe and Si as the inner helix, (c) Perpendicular view to the < 111 > axis. Fe atoms are in brown; Si atoms are in blue.

$P2_13$), which exhibits a close structural relationship with the diamond structure [10]. Fe and Si atoms both occupy the 4*a* sites in the cubic unit cell forming a distorted three-dimensional diamond network with chirality. A body diagonal view (< 111 > direction) shows the triangular patterns with alternation of the Fe and Si arrangement (Fig. 1*a*). A perpendicular view of the < 111 > direction (Fig. 1*c*) reveals that FeSi consists of two Fe and Si intertwined 3-fold helices with an additional, smaller, 3-fold helix embedded in the middle. The nature of the internal helix (Fe or Si) alternates between neighboring helices (Fig. 1b), but the interatomic distances remain comparable (2.75 Å for Fe, 2.78 Å for Si). Neighboring helices are interconnected, with every atom constituting the outside helices being shared between six different units. FeSi forms a category of its own as many compounds adopt the same primitive cubic structure with intertwined helices and exhibit a variety of properties, including the Kondo insulator behavior seen in FeSi [2], the skyrmion lattice structure discovered in FeGe [31,32], $Fe_{1-x}Co_xSi$, MnGe, and MnSi [13,33], the diamagnetic semi-metal behavior in CoSi [34], and heavy Fermion metal/Kondo insulator behavior seen in $FeSi_{1-x}Al_x$ [35]. While doping or substitution of both the iron and silicon sites in FeSi has drawn significant interest, the structure of FeSi also offers the possibility of intercalating atoms in empty sites. With the idea of expanding on the FeSi framework arrangement, we shifted our focus onto FeSi-containing 111-type phases and related compounds. According to the ICSD database, the vast majority of the reported equiatomic ternary iron silicides such as LaFeSi [36], NbFeSi [18], and NiFeSi [37] (Fig. 2) adopt one of three centrosymmetric structures: PbClF, TiNiSi or Co_2Si- types with TiFeSi being an exception. The DOS of the three compounds previously cited show that, in all cases, the area around the Fermi level is dominated by the transition metal, Fe, with a relatively high DOS indicating the metallic and potentially magnetic properties of the different phases. The PbClF-type structure adopted by the lanthanide iron silicides (and Yttrium) exhibits a layered structure with edge-sharing $FeSi_4$ tetrahedra. This structure has been of interest recently with the emergence of the superconducting hydride LaFeSiH [38]. As we move to less electropositive elements, the layered character of the PbClF-type structure is lost with the formation of edge sharing four- and eight-rings. As a result, the electron count referred to from that point onwards takes into consideration the *s* and *d* valence electrons of the different metals present in the compounds (as well as the *p* electrons for Si). Iron silicides with a lower electron count (15–17 e-/f.u.), containing U, Sc and early transition metals (Zr, Hf, Ta, and Nb) join the large TiNiSi family of compounds and those containing Co and Ni (21 and 22 e-/f.u.) adopt a variation of the structure, the Co_2Si-type [37]. However, none of these compounds are supposed to favor the helical magnetic behavior in FeSi-type compounds because of the presence of an inversion center [37,39]. As an effort to investigate the magnetic ordering in FeSi containing structures, the non-centrosymmetric compound TiFeSi (S.G. *Ima*2) [20] was preferred for this study.

3.1.1. Phase analysis and structural comparison of hexagonal and orthorhombic structures of TiFeSi

TiFeSi was successfully synthesized using an arc-melting approach. An elemental analysis by SEM-EDS gave the chemical composition of $Ti_1Fe_{1.0(1)}Si_{0.9(1)}$ for both hexagonal and orthorhombic phases. The powder pattern presented in Fig. 3*a* showed evidence the orthorhombic phase was present in the sample as expected from the reported TiFeSi compound [20]. However, the Le Bail fitting of the powder diffraction patterns indicates the multiple phases exist in TiFeSi. One can also observe the absence of peak splitting at 44° 2θ, which is expected for the orthorhombic phase for the (013) and (042)/(051) reflections, but rather a peak broadening of the (012) reflection of the hexagonal phase. Additionally, the relative intensities of the peaks around 52° are not in agreement with those of the orthorhombic phase. To confirm the existence of the hexagonal phase, we performed the powder XRD measurement on as-cast TiFeSi using beamline 11-BM at the Advanced Photon Source, Argonne National Laboratory. The refined powder XRD pattern shown in Fig. 3*d* clearly demonstrates ~60% of the sample crystallizes in the hexagonal structure. Based on the superlattice relationship between the Fe_2P-type and the TiFeSi-type, a volume optimization was designed and carried out for both the orthorhombic and hexagonal structures of TiFeSi. The structure of the Fe_2P-type was used as a starting point for the optimization of the hexagonal phase for our compound. After fitting both curves with the Birch-Murnaghan equation of state (Fig. S1), it appears that the orthorhombic structure is always energetically favored, therefore making it the preferred configuration. However, the energy gap between the two curves at the optimal volume for both phases is only ~0.2 meV per atom. Therefore, it can be speculated that a phase transition between the orthorhombic and hexagonal

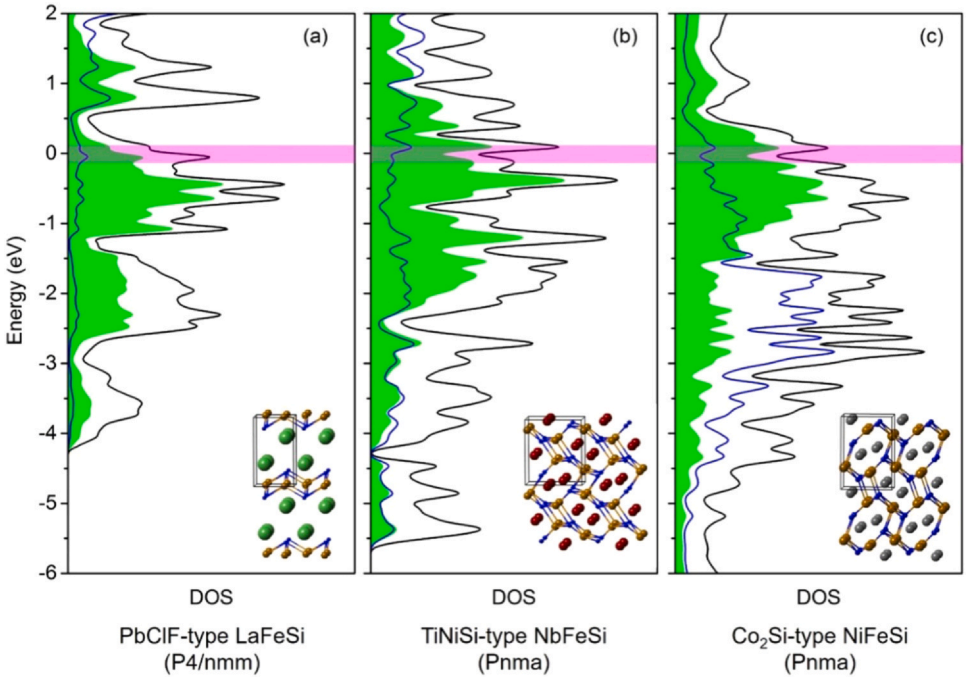

Fig. 2. Crystal structures and density of states (DOS) of AFeSi compounds with (a) LaFeSi, (b) NbFeSi, and (c) NiFeSi. Fe–Si bonds are highlighted. The total DOS is in black while partial DOS of Fe is in green. The partial DOS of the A element is also presented, in blue. (For interpretation of the references to colour in this figure legend, the reader is referred to the web version of this article.)

structures might be reached with a temperature variation, which was further investigated experimentally.

3.2. Structure determination of hexagonal TiFeSi

Both experimental and theoretical observations drove us to investigate the crystal structure using single crystal X-ray diffraction. The study showed the presence of two distinct phases, the expected orthorhombic structure with space group *Ima*2 (S.G.46) and a secondary phase of the hexagonal structure with space group *P*-62*m* (S.G.189). In the past, TiFeSi was described as a superstructure of the ordered Fe_2P-type [20]. Nonetheless, this present report shows a structure with higher symmetry is also attainable. The detailed crystallographic data is presented in Tables 1 and 2. The refined hexagonal phase is comparable with Fe_2P with Si atoms located at the 2*c* and 1*b* site corresponding to the P sites in Fe_2P and Fe and Ti occupying the tetrahedral 3*f* and square pyramidal 3*g* sites, respectively. The flexible refinements on each site have been tested to verify the vacancies in the hexagonal TiFeSi structure. According to the results, no vacancies were observed. The high isotropic displacement parameters obtained during the refinement, in particular that of Si2, are consistent with the instability of the hexagonal structure. As a matter of fact, when looking at the sites occupied by Si atoms in the orthorhombic structure [20], the atoms are slightly shifted from their ideal positions to adopt a more thermodynamically stable structure. As a result, the unit cell rearranges itself from hexagonal to orthorhombic. The structure of the hexagonal phase is shown in Fig. 4 in comparison with the orthorhombic structure. The clear periodicity of the atomic arrangement in the hexagonal structure leads to the very straight alternation of Fe and Ti layers. This is in opposition with the staggered/shifted arrangement of the atoms in the orthorhombic structure. As mentioned previously, the orthorhombic phase can be regarded as a superlattice of the hexagonal structure as shown by the highlighted red unit cell of the orthorhombic structure in comparison to the purple unit cell of the tetragonal one. Corresponding anisotropic displacement parameters and significant interatomic distances are summarized in Tables S1 and S2. Each Fe atom forms four bonds with adjacent Si atoms creating layers of $FeSi_4$ tetrahedra with Ti atoms present in the empty site between them (with a total of 11 neighboring atoms). The short Fe–Fe distances (2.691(8) Å and 2.709(9) Å for the orthorhombic structure and 2.671(4) Å for hexagonal one) form isolated Si-containing triangular planar patterns as highlighted in Fig. 4, which could potentially lead to a frustrated magnetic state.

3.3. Structure determination and magnetic behavior of orthorhombic α-TiFeSi

Efforts were made to obtain a pure hexagonal phase for TiFeSi. Annealing the as-cast sample at 1000 °C for seven days yields the low-temperature orthorhombic phase while a repeated arc-melting process led to the high-temperature hexagonal phase as the majority phase, however, evidence for the presence of the orthorhombic phase was still observed in the powder pattern. The structure refinement carried out on the single crystal diffraction data was in agreement with the phase reported by Jeitschko [20].

Motivated by our original goal of obtaining new helical magnetic behavior, we conducted a series of magnetic measurements to investigate the behavior of the non-centrosymmetric compound. All the magnetic measurements were conducted on the pure orthorhombic TiFeSi sample. The magnetic susceptibility (χ) as a function of temperature (T) is plotted in Fig. 5a. The zero-field cooled (ZFC) and field cooled (FC) data obtained at 1 T overlap each other without giving any obvious information about the magnetic ordering. The high temperature part of the susceptibility (χ_0) was subtracted to minimize the external impurity effect. The reciprocal susceptibility ($1/\chi_m$ with $\chi_m = \chi - \chi_0$) is presented in the Inset of Fig. 5*a*. The linear fit shows that the compound exhibits a Curie-Weiss behavior at high temperatures (T > 250 K) with a positive Weiss temperature of $\theta = 99$ K and effective moment $\mu_{eff} = 0.63\ \mu_B$/f.u., which indicates weak ferromagnetic interactions are present in the sample. The M (H) data at 5 K, 200 K, and 300 K are shown in Fig. 5*b*. The paramagnetic behavior drawn from the linear fitting is confirmed at

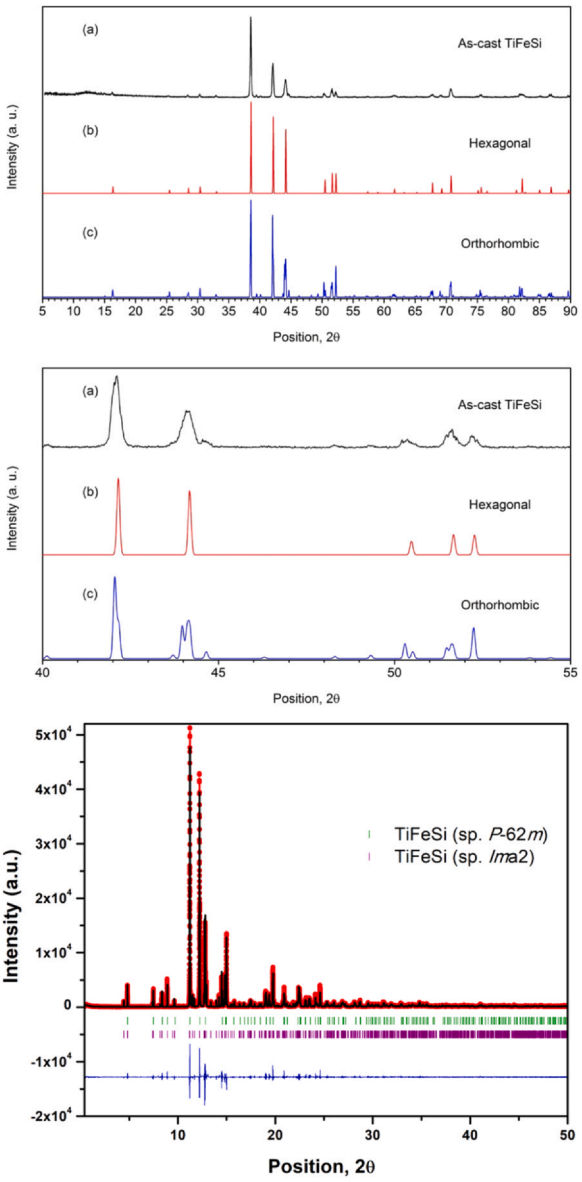

Fig. 3. XRD pattern of (a) as-cast TiFeSi sample and calculated patterns for (b) hexagonal and (c) orthorhombic TiFeSi structures. The bottom graph should a close-up of the 2θ range 40–55°. (d) Rietveld refinement of TiFeSi with the coexistence of orthorhombic and hexagonal phases.

Table 1
Single crystal crystallographic data for hexagonal, β-TiFeSi at 300 (2) K.

Refined formula	β-TiFeSi
F.W. (g/mol)	131.84
Space group; Z	*P*-62*m*(No.189); 3
a (Å)	6.257(2)
c (Å)	3.497(1)
V (Å^3)	118.55(9)
Absorption Correction	Numerical
Extinction Coefficient	0.04(2)
θ range (deg)	3.760–32.035
hkl ranges	$-9 \le h,k \le 9$ $-5 \le l \le 5$
No. reflections; R_{int}	1410; 0.0367
No. independent reflections	182
No. parameters	15
R_1: ωR_2 (all *I*)	0.0385; 0.0755
Goodness of fit	1.356
Diffraction peak and hole (e$^-$/ Å^3)	0.836; − 1.482

Table 2
Atomic coordinates and equivalent isotropic displacement parameters of the β-TiFeSi system (U_{eq} is defined as one-third of the trace of the orthogonalized U_{ij} tensor (Å^2)).

Atom	Wyckoff.	Occ.	*x*	*y*	*z*	U_{eq}
Ti	3*g*	1	0	0.4219(5)	½	0.0142(6)
Fe	3*f*	1	0.7535(3)	0	0	0.0212(6)
Si1	2*c*	1	⅔	⅓	0	0.0055(8)
Si2	1*b*	1	0	0	½	0.045(3)

300 K but also present at 200 K. The M (H) curve at 5 K shows no hysteresis but exhibits a larger slope at lower fields in contrast with the linear behavior at higher fields (~ > 1 T). Additionally, saturation was not reached throughout the whole field range, consistent with a weakly ferromagnetic ordered state. A change of slope can be observed around 60 K, which is a sign of an additional transition in the system. Given the small value of the non-saturating ordered moment and positive Weiss temperature, the system most likely has a weak helimagnetic order at low temperatures [40]. The minimum in the magnetization derivative around 60 K ($dM/dT < 0$) shown in the Supporting Information (Fig. S2) is consistent with the magnetic ordering. AC susceptibility measurements were carried out to further investigate the nature of the transition below 100 K under a 10 Oe field. The results at different frequencies (100, 500 and 5000 Hz) are shown in Fig. S3 for the imaginary component, χ". No shift of the transition temperature is observed ruling out the possibility of spin-glass transition. The results further support the possible presence of a helical magnetic structure as a result of the competition between the ferromagnetic and antiferromagnetic interactions in the sample, although simple antiferromagnetism cannot be ruled out.

To gain further insight into the stability of the hexagonal structure of TiFeSi, the electronic density of states (DOS) was simulated for both the hexagonal and orthorhombic structures with optimized lattice parameters. The total and partial DOS for both structures were obtained through a non-spin polarized local density approximation (LDA) and are presented in Fig. S4. The partial DOS reveal the high contribution from the Fe states located in the top of the bonding states just below and right above the E_F while Ti greatly contributes to the antibonding states above at higher energy levels (> 0.5 eV). Si atoms show little contribution to the total DOS around the Fermi level. The lower-lying states (− 6 to − 2 eV) are a combination of Ti, Fe and Si contributions. As a result of the experimental results supporting the idea of helimagnetism at low *T*, no further calculations were carried out due to the lack of a reliable magnetic model at this time for accurate simulations.

3.3.1. Magnetic behavior and electronic structures of MFeSi (M = Zr and Hf)

To compare the behavior of TiFeSi with related compounds, we extended our studies to MFeSi (M = Zr and Hf). Theoretical calculations were carried out on the two centrosymmetric silicide compounds. The total energies of five different models including nonmagnetic (NM), ferromagnetic (FM), and antiferromagnetic (AFM) patterns of MFeSi (M = Zr and Hf) are listed in Table 3 relative to the lowest energy case model AFM3. The different spin orientations are pictured below. We used these relative total energies to estimate the magnetic ordering among the five different magnetic ordering schemes as a function of temperature using a Boltzmann distribution. The calculations clearly indicate that an antiferromagnetic ordering is preferred by both ZrFeSi and HfFeSi. The non-magnetic pattern is clearly disfavored with the highest total energy out of the five models investigated. A closer look at the spin orientation reveals the preference for an antiferromagnetic distribution with respect to the two shortest Fe–Fe interactions (model AFM3). Due to the very small difference between the longest Fe–Fe distances (4.283 vs

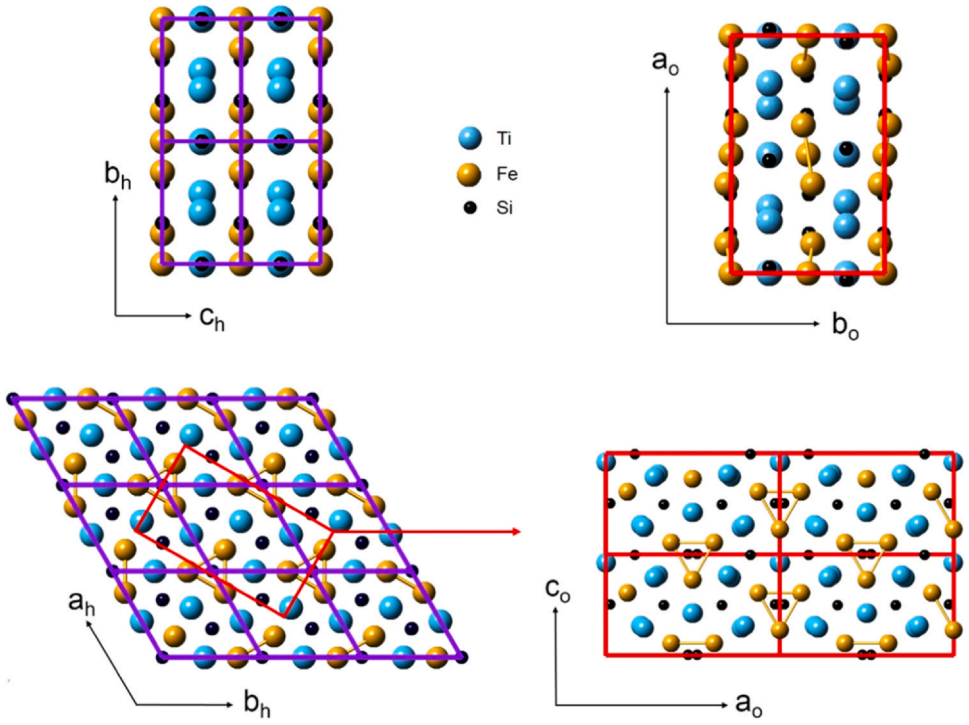

Fig. 4. Comparison of the (Left) hexagonal β- and (Right) orthorhombic α- structures of TiFeSi. The unit cells are represented in purple and red to highlight the relationship between the two structures respect the proportion between the length of *a*, *b* and *c* of the two sets. The Fe–Fe bonds create isolated triangles in the structure. (For interpretation of the references to colour in this figure legend, the reader is referred to the web version of this article.)

4.212 Å for Zr, 4.267 vs 4.120 Å for Hf) the model AFM2 is very close in energy, with only a 23.9 and 38.7 meV/f.u. difference with the AFM3 model for Zr and Hf, respectively. Both the ferromagnetic (FM) and the third column antiferromagnetic (AFM1) models present a ferromagnetic coupling for the shortest Fe–Fe distance, which is not favored as indicated by the higher total energies.

While the spin orientation shows some ferromagnetic arrangement of the spins, one could argue that the atomic distances between the concerned iron atoms are too large to be considered significant in terms of bonding and magnetic interactions. If we disregard the long Fe–Fe distances and expand the view to several unit cells (Table 3), we notice that the iron atoms form infinite zigzag chains along the y axis. When adding the spin orientation of the AFM3 model determined previously, one can fully appreciate the antiferromagnetic ordering along the zigzag chains that prevails in the compound. The total DOS curves are shown along with the partial DOS for the Fe atoms in both the non-magnetic and antiferromagnetic models in Fig. S5. The DOS obtained for the Zr and Hf compounds are very comparable throughout the entire energy range studied. Contributions from Fe dominate the DOS over the entire energy range confirming the origin of the magnetism coming mostly from the iron present in the structure.

To further verify the computational results, both ZrFeSi and HfFeSi were synthesized through a high-temperature arc melting approach. Details on the synthesis and phase identification (Fig. S6) are given in the Supplementary Information. The magnetic susceptibility and variation of the magnetization as function of field are presented in Fig. S7. For ZrFeSi (Fig. S7a) two broad magnetic

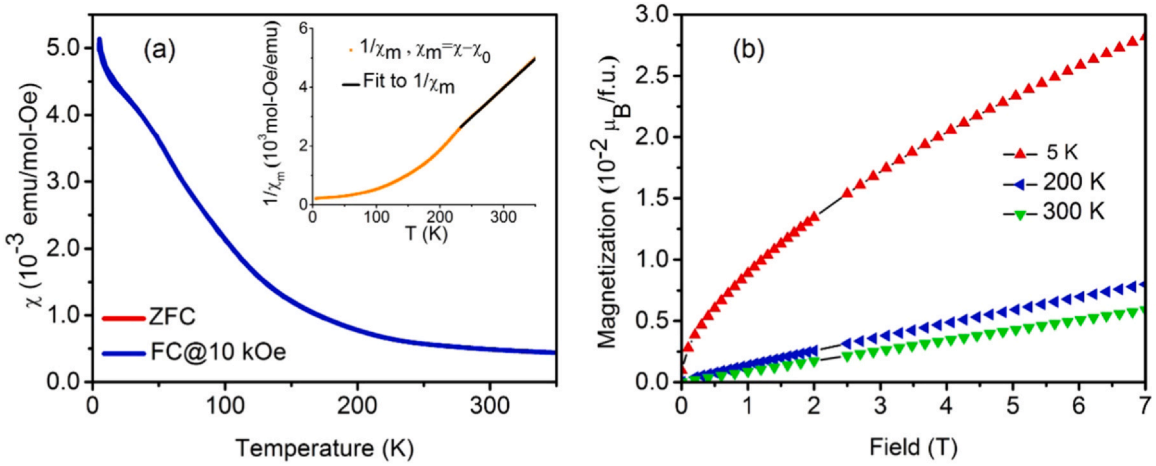

Fig. 5. Magnetic properties of Orthorhombic phase of TiFeSi: (a) Magnetic susceptibility as function of temperature for zero field cooled (ZFC) and field cooled (FC) condition at 10 kOe. Inset shows inverse of modified susceptibility ($\chi_m = \chi - \chi_0$) as function of temperature (T). The black line represents straight line fitting: $1/\chi_m = C/(T-\theta)$, where C is Curie constant and θ is Weiss temperature. $\chi_0 = 2.97.10^{-4}$ is the obtained initially by fitting high temperature susceptibility with modified Curie-Weiss law. $\chi = \chi_0 + C'/(T-\theta')$.

Table 3
Relative total energies (ΔE in meV/f.u. and K/f.u.) calculated for different magnetic models with respect to the lowest energy model in ZrFeSi and HfFeSi by Wien2k with spin-orbital coupling.

	ΔE	NM	FM	AFM1	AFM2	AFM3
ZrFeSi	meV/f.u.	502.8	70.3	102.5	23.9	0
	K/f.u.	5830	815	1189	277	0
HfFeSi	meV/f.u.	366.4	97.3	92.8	38.7	0
	K/f.u.	4250	1129	1076	449	0

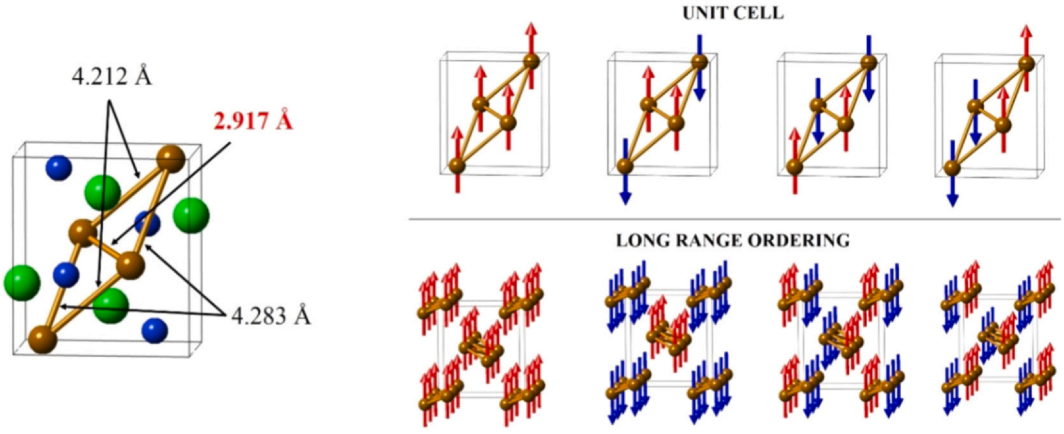

(NM: NonMagnetic; FM: FerroMagnetic; AFM: AntiFerroMagnetic). The bond distances are given for the Zr sample.

transitions can be observed around 250 K and 80 K respectively where the magnetization drops in the range 80 K < T < 250 K with a slight upturn below 80 K. HfFeSi (Fig. S7c) also exhibits two magnetic transitions around 180 K and 60 K qualitatively similar to ZrFeSi although the susceptibility values differ by one order of magnitude. For ZrFeSi (Fig. S7c), the M(H) curve looks similar with a small low field ferromagnetic component at all temperatures even up to 300 K. Again, this is likely due to a small amount of a ferromagnetic impurity phase. In the case of HfFeSi (Fig. S7d), there also seems to be relatively small ferromagnetic component even at low temperature.

With the current data we cannot predict the exact nature of the magnetism in either of these samples except that TiFeSi seems to have a weak helimagnetic order below 100 K. Neutron diffraction measurements on single crystal samples will be necessary for such a determination. The presence of impurities in the ZrFeSi sample could very likely be the origin of the ferromagnetic behavior observed at low temperature and high field. However, the overall antiferromagnetic behavior exhibited by the sample is in agreement with the results of the calculations, which demonstrates the difference between the centrosymmetric compounds MFeSi (M=Zr, Hf) and non-centrosymmetric TiFeSi.

4. Conclusions

The new β-TiFeSi phase, with a hexagonal structure *P*-62*m* (S.G.189), was successfully obtained by a high temperature method using an arc-melting approach. The stability of the phase was investigated using volume optimization and DOS calculations in comparison with the previously reported orthorhombic phase. While a pure hexagonal phase could not be attained, magnetic measurements were conducted on the pure orthorhombic phase obtained through annealing. The magnetic measurements showed evidence of weak ferromagnetic interactions present in the sample with a modified Curie-Weiss behavior at higher temperatures. Low temperature measurements show the presence of a magnetic transition and the M (H) data suggests the possible presence of helical magnetism as observed in other non-centrosymmetric compounds related to the FeSi structure. Future efforts will be focused on the single crystal synthesis in order to further explore the possibility of helimagnetism and possible skyrmion lattice in TiFeSi. As an effort to compare centrosymmetric and non-centrosymmetric compounds, the magnetic behavior of MFeSi (M = Zr and Hf) was simulated leading a favored antiferromagnetic model that was confirmed experimentally.

CRediT authorship contribution statement

Madalynn Marshall: Data analysis, Writing - review & editing; **Jasmine Sanford under the guidance of Dr. Lea Gustin:** Synthesis of the materials and characterization; **William Shelton:** Theoretical calculation. **Weiwei Xie:** Supervision, Propose the research, Physical properties measurement and Data analysis, Partial calculation, Writing - review & editing, Funding acquisition.

Declaration of Competing Interest

The authors declare that they have no known competing financial interests or personal relationships that could have appeared to influence the work reported in this paper.

Acknowledgments

W.X. appreciates the significant contribution from Dr. Lea Gustin and useful discussion with Prof. John DiTusa and Prof. David Young. The work in the Xie group is supported by the Beckman Young Investigator Award and NSF-DMR-2053287. The SEM-EDS and magnetic measurements were conducted at the Shared Instrument Facility (SIF), Louisiana State University. Magnetic measurements

were supported by the U.S. Department of Energy under the Experimental Program to Stimulate Competitive Research (EPSCoR) Grant No. DESC0012432, with additional support from the Louisiana Board of Regents. Use of the Advanced Photon Source at Argonne National Laboratory was supported by the U. S. Department of Energy, Office of Science, Office of Basic Energy Sciences, under Contract No. DE-AC02-06CH11357.

Appendix A. Supporting information

Supplementary data associated with this article can be found in the online version at doi:10.1016/j.jallcom.2021.158617.

References

[1] D. Mandrus, J.L. Sarrao, A. Migliori, J.D. Thompson, Z. Fisk, Thermodynamics of FeSi, Phys. Rev. B 51 (1995) 4763–4767.
[2] J.F. DiTusa, K. Friemelt, E. Bucher, G. Aeppli, A.P. Ramirez, Metal-insulator transitions in the Kondo insulator FeSi and classic semiconductors are similar, Phys. Rev. Lett. 78 (1997) 2831–2834.
[3] J. Beille, J. Voiron, M. Roth, Long period helimagnetism in the cubic B20 $Fe_xCo_{1-x}Si$ and $CoxMn_{1-x}$ Si alloys, Solid State Commun. 47 (1983) 399–402, https://doi.org/10.1016/0038-1098(83)90928-6
[4] W. Münzer, A. Neubauer, T. Adams, S. Mühlbauer, C. Franz, F. Jonietz, R. Georgii, P. Böni, B. Pedersen, M. Schmidt, A. Rosch, C. Pfleiderer, Skyrmion lattice in the doped semiconductor $Fe_{1-x}Co_xSi$, Phys. Rev. B 81 (2010) 041203, https://doi.org/10.1103/PhysRevB.81.041203
[5] S.X. Huang, F. Chen, J. Kang, J. Zang, G.J. Shu, F.C. Chou, C.L. Chien, Unusual magnetoresistance in cubic B20 $Fe_{0.85}Co_{0.15}Si$ chiral magnets, New J. Phys. 18 (2016) 065010, https://doi.org/10.1088/1367-2630/18/6/065010
[6] C. Pfleiderer, T. Adams, A. Bauer, W. Biberacher, B. Binz, F. Birkelbach, P. Böni, C. Franz, R. Georgii, M. Janoschek, F. Jonietz, T. Keller, R. Ritz, S. Mühlbauer, W. Münzer, A. Neubauer, B. Pedersen, A. Rosch, Skyrmion lattices in metallic and semiconducting B20 transition metal compounds, J. Phys. Condens. Matter 22 (2010) 164207, https://doi.org/10.1088/0953-8984/22/16/164207
[7] N. Nagaosa, Y. Tokura, Topological properties and dynamics of magnetic skyrmions, Nat. Nano 8 (2013) 899–911.
[8] A. Fert, V. Cros, J. Sampaio, Skyrmions on the track, Nat. Nano 8 (2013) 152–156, https://doi.org/10.1038/nnano.2013.29
[9] X. Yu, J.P. DeGrave, Y. Hara, T. Hara, S. Jin, Y. Tokura, Observation of the magnetic skyrmion lattice in a MnSi nanowire by Lorentz TEM, Nano Lett. 13 (2013) 3755–3759, https://doi.org/10.1021/nl401687d
[10] W. Xie, S. Thimmaiah, J. Lamsal, J. Liu, T.W. Heitmann, D. Quirinale, A.I. Goldman, V. Pecharsky, G.J. Miller, β-Mn-Type $Co_{8+x}Zn_{12-x}$ as a defect cubic laves phase: site preferences, magnetism, and electronic structure, Inorg. Chem. 52 (2013) 9399–9408, https://doi.org/10.1021/ic4009653
[11] Y. Tokunaga, X.Z. Yu, J.S. White, H.M. Rønnow, D. Morikawa, Y. Taguchi, Y. Tokura, A new class of chiral materials hosting magnetic skyrmions beyond room temperature, Nat. Commun. 6 (2015) 7638, https://doi.org/10.1038/ncomms8638
[12] K. Karube, J.S. White, N. Reynolds, J.L. Gavilano, H. Oike, A. Kikkawa, F. Kagawa, Y. Tokunaga, H.M. Ronnow, Y. Tokura, Y. Taguchi, Robust metastable skyrmions and their triangular-square lattice structural transition in a high-temperature chiral magnet, Nat. Mater. 15 (2016) 1237–1242.
[13] S. Mühlbauer, B. Binz, F. Jonietz, C. Pfleiderer, A. Rosch, A. Neubauer, R. Georgii, P. Böni, Skyrmion lattice in a chiral magnet, Science 323 (2009) 915–919, https://doi.org/10.1126/science.1166767
[14] D. McGrouther, R.J. Lamb, M. Krajnak, S. McFadzean, S. McVitie, R.L. Stamps, A.O. Leonov, A.N. Bogdanov, Y. Togawa, Internal structure of hexagonal skyrmion lattices in cubic helimagnets, New J. Phys. 18 (2016) 095004, https://doi.org/10.1088/1367-2630/18/9/095004
[15] T. Graf, C. Felser, S.S.P. Parkin, Simple rules for the understanding of Heusler compounds, Prog. Solid State Chem. 39 (2011) 1–50, https://doi.org/10.1016/j.progsolidstchem.2011.02.001
[16] R. Gautier, X. Zhang, L. Hu, L. Yu, Y. Lin, O.L. SundeTor, D. Chon, K.R. Poeppelmeier, A. Zunger, Prediction and accelerated laboratory discovery of previously unknown 18-electron ABX compounds, Nat. Chem. 7 (2015) 308–316.
[17] J.T. Zhao, E. Parthé, Ternary equiatomic hafnium-transition metal suicides, J. Common Met. 163 (1990) L7–L12, https://doi.org/10.1016/0022-5088(90)90605-J
[18] W. Jeitschko, A.G. Jordan, P.A. Beck, V and E phases in ternary systems with transition metals and silicon or germanium, Trans. Metall. Soc. AIME 245 (1969) 335–339.
[19] J. Gayles, F. Freimuth, T. Schena, G. Lani, P. Mavropoulos, R.A. Duine, S. Blügel, J. Sinova, Y. Mokrousov, Dzyaloshinskii-Moriya interaction and hall effects in the skyrmion phase of $Mn_{1-x}Fe_xGe$, Phys. Rev. Lett. 115 (2015) 036602, https://doi.org/10.1103/PhysRevLett.115.036602
[20] W. Jeitschko, The crystal structure of TiFeSi and related compounds, Acta Crystallogr. Sect. B 26 (1970) 815–822, https://doi.org/10.1107/S0567740870003163
[21] M.B. Gamża, W. Schnelle, H. Rosner, S.-V. Ackerbauer, Yu Grin, A. Leithe-Jasper, Complex magnetic phase diagram of metamagnetic MnPtSi, Phys. Rev. B 100 (2019) 014423, https://doi.org/10.1103/PhysRevB.100.014423
[22] J. Rodríguez-Carvajal, Recent advances in magnetic structure determination by neutron powder diffraction, Phys. B 192 (1993) (1993) 55–69, https://doi.org/10.1016/0921-4526(93)90108-I
[23] Bruker, SMART, Bruker AXS Inc., Madison, Wisconsin, USA, 2012.
[24] G.M. Sheldrick, A short history of *SHELX*, Acta Crystallogr. A 64 (2008) 112–122, https://doi.org/10.1107/S0108767307043930
[25] P. Blaha, K. Schwarz, G.K.H. Madsen, D. Kvasnicka, J. Luitz, WIEN2K, An Augmented Plane Wave + Local Orbitals Program for Calculating Crystal Properties, Karlheinz Schwarz, Techn. Universität Wien, Austria, Wien, Austria, 2001.
[26] F. Birch, Finite elastic strain of cubic crystals, Phys. Rev. 71 (1947) 809–824, https://doi.org/10.1103/PhysRev.71.809
[27] P.E. Blöchl, Projector augmented-wave method, Phys. Rev. B 50 (1994) 17953–17979.
[28] J.P. Perdew, K. Burke, M. Ernzerhof, Generalized gradient approximation made simple, Phys. Rev. Lett. 77 (1996) 3865–3868, https://doi.org/10.1103/PhysRevLett.77.3865
[29] U. von Barth, L. Hedin, A local exchange-correlation potential for the spin polarized case. i, J. Phys. C Solid State Phys. 5 (1972) 1629–1642, https://doi.org/10.1088/0022-3719/5/13/012
[30] H.J. Monkhorst, J.D. Pack, Special points for Brillouin-zone integrations, Phys. Rev. B 13 (1976) 5188–5192, https://doi.org/10.1103/PhysRevB.13.5188
[31] X.Z. Yu, N. Kanazawa, Y. Onose, K. Kimoto, W.Z. Zhang, S. Ishiwata, Y. Matsui, Y. Tokura, Near room-temperature formation of a skyrmion crystal in thin-films of the helimagnet FeGe, Nat. Mater. 10 (2011) 106–109, https://doi.org/10.1038/nmat2916
[32] C. Wang, H. Du, X. Zhao, C. Jin, M. Tian, Y. Zhang, R. Che, Enhanced stability of the magnetic skyrmion lattice phase under a tilted magnetic field in a two-dimensional chiral magnet, Nano Lett. (2017), https://doi.org/10.1021/acs.nanolett.7b00135
[33] R. Ritz, M. Halder, M. Wagner, C. Franz, A. Bauer, C. Pfleiderer, Formation of a topological non-Fermi liquid in MnSi, Nature 497 (2013) 231–234, https://doi.org/10.1038/nature12023
[34] J.H. Wernick, G.K. Wertheim, R.C. Sherwood, Magnetic behavior of the monosilicides of the 3d-transition elements, Mater. Res. Bull. 7 (1972) 1431–1441.
[35] J.F. DiTusa, K. Friemelt, E. Bucher, G. Aeppli, A.P. Ramirez, Heavy fermion metal–Kondo insulator transition in $FeSi_{1-x}Al_x$, Phys. Rev. B 58 (1998) 10288–10301.
[36] R. Welter, I. Ijjaali, G. Venturini, B. Malaman, X-Ray single crystal refinements on some CeFeSi-type RTX compounds (R = RE elements; T = Mn, Fe, Co, Ru; X = Si, Ge).: Evolution of the chemical bonds, J. Alloy. Compd. 265 (1998) 196–200.
[37] G.A. Landrum, R. Hoffmann, J. Evers, H. Boysen, The TiNiSi family of compounds: structure and bonding, Inorg. Chem. 37 (1998) 5754–5763, https://doi.org/10.1021/ic980223e
[38] F. Bernardini, G. Garbarino, A. Sulpice, M. Núñez-Regueiro, E. Gaudin, B. Chevalier, A. Cano, S. Tencé, Iron-based superconductivity extended to the novel hydride LaFeSiH, ArXiv170105010 Cond-Matsupr-Con. (2017). https://arxiv.org/abs/1701.05010 (Accessed April 21, 2017).
[39] V. Johnson, W. Jeitschko, Ternary equiatomic transition metal silicides and germanides, J. Solid State Chem. 4 (1972) 123–130, https://doi.org/10.1016/0022-4596(72)90140-5
[40] C. Dhital, M.A. Khan, M. Saghayezhian, W.A. Phelan, D.P. Young, R.Y. Jin, J.F. DiTusa, Effect of negative chemical pressure on the prototypical itinerant magnet MnSi, Phys. Rev. B. 95 (2017) 024407, https://doi.org/10.1103/PhysRevB.95.024407